

Simulation of cryovolcanism on Saturn's moon Enceladus with the Green-Naghdi theory of thermoelasticity

Swantje BARGMANN^{1*}, Ralf GREVE² and Paul STEINMANN^{1**}

¹ Chair of Applied Mechanics, University of Kaiserslautern, P.O. Box 3049, 67653 Kaiserslautern, Germany

² Institute of Low Temperature Science, Hokkaido University, Kita-19, Nishi-8, Kita-ku, Sapporo 060-0819, Japan

(Received April 7, 2008; Revised manuscript accepted August 10, 2008)

Abstract

In 2005, the Cassini spacecraft proved the existence of cryovolcanism, *i.e.*, the icy counterpart of volcanism on Earth, on Saturn's moon Enceladus during its close fly-bys. In particular, water-rich plume venting was discovered in the south polar region. Thus, Enceladus was found to be one out of three outer solar bodies to be geologically active. This contribution is concerned with the modelling and computation of this phenomenon. For the underlying thermoelastic description of ice at cryogenic temperatures, we resort to the Green-Naghdi approach. The Green-Naghdi theory includes the classical Fourier approach, but, in addition to that, it is a lot more general as it also allows for other types of heat propagation. The numerical implementation is carried out with the help of the finite element method. Results show that lateral spreading of internal and surface warming away from an active volcanic vent increases strongly with increasing contribution of the non-classical heat flux. Agreement with available high-resolution surface temperature data based on infrared spectrometry seems to be best if the non-classical heat flux contributes significantly to the total heat transport. Complementary laboratory studies would be required in order to strengthen this speculative, yet promising idea.

1. Introduction

Enceladus is one of Saturn's inner satellites. It was discovered in 1789 and orbits Saturn in an almost circular orbit with a semi-major axis of 237,948 km and a period of 1.37 days. Enceladus has the shape of a flattened ellipsoid with a mean diameter of 504 km, which makes it the sixth-largest Saturnian moon. It consists of a rocky core and an icy mantle and surface, the mean surface temperature being at a cryogenic value of 77 K. In many ways, the general properties of Enceladus are very different from those of other satellites, and thus, it is a very active research topic. With an albedo of 0.99, it has the most reflective surface of any body in the solar system. Moreover, it shows recent geological activity, which is very unusual for such a small body.

Of particular interest is Enceladus' south polar region. Active cryovolcanism was found there in 2005 during a fly-by of the Cassini spacecraft (Porco *et al.* 2006), which makes Enceladus the fourth body in the

solar system (along with the Earth, Jupiter's moon Io and Neptune's moon Triton) where volcanic eruptions have been observed. This finding goes along with the spectrometric detection of a distinctive warm spot centered on the south pole with a temperature of approximately 85 K, which is 15 K more than expected from a simple radiation balance (Fig. 1; Spencer *et al.* 2006).

Cryovolcanoes are icy equivalents of the well-known terrestrial volcanoes. Their main features are illustrated in Fig. 2. Instead of magma, Enceladus' cryovolcanoes erupt water, which has its source in pressurized sub-surface water chambers (Porco *et al.* 2006). No ammonia, which would lower the melting point, was found (Buratti *et al.* 1990), suggesting that the cryomagma is pure H₂O. Cryovolcanoes on other icy moons may also erupt a mixture of water and, for example, ammonia or methane.

The exact source which produces the cryovolcanic water plumes is still subject to research. In the literature, different mechanisms have been proposed to explain the plume origin. Collins and Goodman

* Now at Department of Applied Mechanics, Chalmers University of Technology, 41296 Gothenburg, Sweden

** Now at Chair of Applied Mechanics, University of Erlangen-Nuremberg, Egerlandstraße 5, 91058 Erlangen, Germany

(2007) suggest that localized subsurface melting on Enceladus has produced an internal south polar sea, whereas Nimmo *et al.* (2007) ascribe the heat and vapour production to shear heating by tidally driven lateral fault motion. Another possible explanation is given by Kieffer *et al.* (2006), stating that due to tectonic processes, a clathrate reservoir might be the plume's source. In any case, the existence of the cryovolcanic eruptions is undoubted, and the details on their source are not relevant for this study.

Most problems of heat transport in ice, as well as in other common materials, are accurately described by the classical theory developed by Fourier. However, at cryogenic temperatures material behavior can differ greatly from that at room temperature. One of the properties that might change is the way heat propagates. In the course of time, considerations led

to hyperbolic heat transfer equations that are able to model thermal wave propagation and to overcome the paradox of infinite wave speed inherent in Fourier's theory. Among the different approaches which have been suggested, the one of Green and Naghdi (1991) stands out by being very consistent and, most important for our case, very general. They formulated a theory which comprises Fourier's classical law, a non-classical law leading to a hyperbolic heat transfer equation as well as a third type of heat conduction which combines both limits. This theory has proven to be well suited for modelling thermoelastic problems at cryogenic temperatures; see Bargmann and Steinmann (2005, 2006). Consequently, in this study we apply the Green-Naghdi thermoelastic theory to ice in order to simulate the phenomenon of cryovolcanism on Enceladus. We state explicitly that this has so far not been directly supported by laboratory studies or field measurements on ice, so that the study is clearly of a speculative nature and aims at exploring a promising possibility.

In 1991, Green and Naghdi published their thermoelastic approach which is capable of modelling a wider range of phenomena than Fourier's theory. The latter is fully included in the Green-Naghdi approach — however, more possibilities are admitted. Thus, classical problems can be simulated as well as thermoelastic phenomena at low temperatures; see the works of Bargmann and Steinmann (2005, 2006). The theory of Green-Naghdi is introduced in Sect. 2 in order to familiarize the reader with this very general approach. Subsequently, a space-time finite element discretization of the resulting initial boundary value problem is sketched in Sect. 3. This is followed by setting up a simplified model for the material properties, geometry, initial and boundary values of Enceladus' cryovolcanism (Sect. 4). Finally, in Sect. 5, computational results for the temperature evolution in the ice surrounding the cryovolcano are presented and discussed for a number of different scenarios.

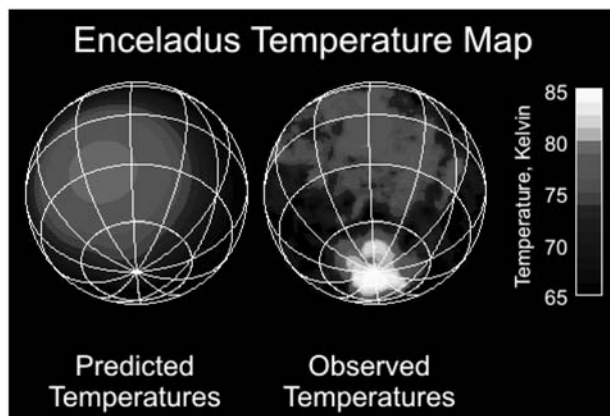


Fig. 1. Predicted (radiation balance) vs. observed (composite infrared spectrometer CIRS onboard the Cassini spacecraft) surface temperatures of Enceladus. The south polar region shows a warm spot due to active cryovolcanism. Credit: NASA/JPL/GSFC.

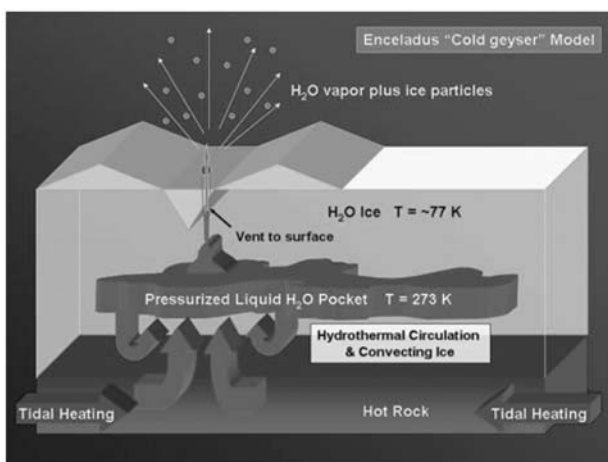


Fig. 2. "Cold geyser model" for cryovolcanism on Enceladus: Pressurized sub-surface water erupts through a volcanic pipe (vent) into the atmosphere. Credit: NASA/JPL/SpaceScience Institute/Cassini-Huygens.

2. Green-Naghdi thermoelasticity

The very general theory developed by Green and Naghdi was only published recently, but a number of studies devoted to its investigation have already been released. Since in this contribution we restrict ourselves to the so-called Green-Naghdi theory of type III (see below), we list only some papers concerning this type in the following. For example, Puri and Jordan (2004) examine the propagation of plane waves in a type-III-thermoelastic continuum. Surface waves in thermoelastic solids are studied by Kumar and Deswal (2001). They apply the theory to an academic example of a micropolar half-space in order to build a basis for the extension to study the role of Green-Naghdi-type surface waves in earth quakes and other geo-

physical applications. Bargmann and Steinmann (2005, 2006, 2008) and Bargmann *et al.* (2008) investigate the general numerical behavior as well as the behavior of temperature profiles of the Green-Naghdi theory.

First, we reiterate the basic ideas of the Green-Naghdi theory in order to introduce its basic properties to the reader. The theory developed by Green and Naghdi (1991) is subdivided into three different types, labeled type I, II and III. The linearized theory of type I is equivalent to Fourier's law, resulting in a parabolic heat equation. In case of type II, no energy dissipation is involved and the resulting heat transfer equation is hyperbolic. Type III is the most general type. It contains both type I and II as limiting cases, thus it is capable of modelling classical Fourier heat conduction as well as undamped thermal wave propagation — and, in addition to that, many more phenomena. The heat flux of type III is an extension of those of type I and II. Both types II and III can overcome the unnatural property of Fourier's law of infinite propagation speed and imply a finite wave propagation speed instead. For modelling cryovolcanism on Enceladus, we apply the universal type III and couple the heat transfer equation with the balance of linear momentum. Type III seems to be the best choice as it is the most general case and includes the other two types.

Thermoelasticity in a finite, isotropic and homogeneous body (an elastic deformable solid) B is considered. First, we summarize the basic concept briefly, since we have already discussed the derivation of the thermal problem in detail in Bargmann and Steinmann (2005), see also Green and Naghdi (1991). Subsequently, the balance of linear momentum is introduced in order to describe the thermomechanical state of body properly.

Green and Naghdi's theory of type III is a very general approach based on the introduction of a scalar quantity α defined by

$$\alpha(\mathbf{X}, t) = \int_{t_0}^t T(\mathbf{X}, \tau) d\tau + \alpha_0, \quad (1)$$

where \mathbf{X} denotes the position vector in the reference configuration, t the time, T the absolute temperature, and α_0 is the initial value of α at the reference time t_0 . α is called thermal displacement, and

$$\dot{\alpha} = T \quad (2)$$

holds, where the dot represents the material time derivative.

At this point, we only state the two equations governing Green-Naghdi thermoelasticity of type III. For a derivation of these equations, the reader is referred to the Appendix. The thermal problem is governed by the heat transfer equation

$$\rho c \dot{T} = \text{div}(k_1 \nabla \alpha) + \text{div}(k_2 \nabla T) + \rho r - 3T_0 \omega K \mathbf{I} : \dot{\boldsymbol{\varepsilon}}, \quad (3)$$

where ρ denotes the constant mass density, c is the non-negative specific heat capacity, $k_{1,2}$ are the non-classical and classical thermal conductivities, respectively, T_0 is the reference temperature, ω the thermal expansion coefficient, K the bulk modulus, \mathbf{I} the unity tensor, r the external heat source and $\boldsymbol{\varepsilon}$ the mechanical strain tensor. Furthermore, the colon operator ($:$) denotes double contraction. The last term in Eq. (3) represents a coupling between the thermal and the mechanical problem, *i.e.*, mechanical strains lead to temperature changes.

The mechanical (deformation) problem is governed by the balance of linear momentum. For geometrically linear deformations, it reads

$$\rho \ddot{\mathbf{u}} = \text{div}(\mathbf{E} : \boldsymbol{\varepsilon} - 3[T - T_0] \omega K \mathbf{I}) + \mathbf{b}, \quad (4)$$

where \mathbf{u} is the mechanical displacement vector, \mathbf{E} the elasticity tensor and \mathbf{b} the volume force. Note that Eq. (4), like Eq. (3), includes a coupling between the thermal and the mechanical problem, so that a fully thermo-mechanically coupled problem is at hand.

3. Finite element discretization

In this section, we shortly describe the chosen discretization method for the initial boundary value problem arising from the Green-Naghdi thermoelasticity described above. The solution method is based on finite elements for the spatial as well as for the temporal problem. Bargmann and Steinmann (2005, 2006) have already shown that this discretization approach suits well for Green-Naghdi thermoelasticity of type III. Those readers who are interested in a mathematical description, we refer to Bargmann and Steinmann (2005, 2006) where we explain the procedure in detail and list all mathematical equations. In the following, only the basic steps are reiterated in order not to repeat everything.

We apply a semi-discretization technique. This means that the spatial and the temporal domain are discretized one after the other. We start with the spatial one and use a standard Bubnov-Galerkin finite element method. The so-called weak form of the equation of interest is one prerequisite. Therefore, the heat transfer equation (3) and the balance of momentum (4) are weighted by test functions and, subsequently, all equations are integrated over the reference configuration B . The unknowns, *i.e.*, the thermal displacement α , the temperature T and the mechanical displacement \mathbf{u} , are interpolated element-wise by the shape functions N^i . Moreover, the test functions are also discretized with the shape functions N^i , according to the Bubnov-Galerkin method. Inserting the approximations results in semi-discretized equations meaning that the nodal values of the unknowns are

now only time-dependent.

After the spatial discretization, we apply a finite element method for the temporal one as well. We resort to a continuous Galerkin time finite element method because it has proved to suit well for Green-Naghdi type III thermoelasticity in the past, see Bargmann and Steinmann (2005, 2006). The reader is also referred to the book of Eriksson *et al.* (1996). The continuous Galerkin method approximates the trial function piecewise and continuously in time by polynomials of degree k . The test functions are approximated piecewise by polynomials of degree $k-1$ which are discontinuous across the element boundaries. The considered time interval $I=[t_0, t_f]$ (t_0 : initial time, t_f : final time) is divided into a finite number of subintervals. In analogy to the spatial finite element method, the weak form is a prerequisite for the discretization process. Thus, we multiply by the temporal test functions and integrate over the corresponding time subinterval. Afterwards, the finite element approximations of the unknowns, *i.e.*, the thermal displacement α , the temperature T and the mechanical displacement \mathbf{u} , and those of the test functions are inserted into the system of equations. As a result, we obtain a fully discrete algebraic set of equations.

We seek for the temporal weak form of the semi-discrete equations on one time subinterval after the other. The solution of the preceding subinterval is used as an initial condition for the current one. In each time step, the coupled system is solved monolithically.

4. Set-up for modelling cryovolcanism on Enceladus

First, the material parameters for cryogenic ice on Enceladus are introduced — followed by the description of the computational domain, the initial and the boundary conditions.

4.1 Model parameters for cryogenic ice

According to Powell (1958), Slack (1980) and Greve (2006), the thermal conductivity, the thermal expansion coefficient and the specific heat capacity of ice are

$$\begin{aligned} k(T) &= \frac{615}{T} \text{Wm}^{-1}\text{K}^{-1}, \\ \omega(T) &= [56.5 + 0.25[T - 273]] \times 10^{-6} \text{K}^{-1}, \\ c(T) &= [146.3 + 7.253T] \text{Jkg}^{-1}\text{K}^{-1}, \end{aligned} \quad (5)$$

where the temperature T is taken in units of [K]. Natural ice is composed of a large number of individual crystals, and we assume that the orientation distribution is random. Thus, its macroscopic mechanical behavior of the ice is isotropic, and the elasticity tensor \mathbf{E} is fully determined by Young's modulus, $E=10$ GPa, and Poisson's ratio, $\nu=0.33$. Both quantities are assumed to be independent of temperature. For

the ice density, we employ the standard value $\rho=910$ kg m^{-3} . While Buratti *et al.* (1990) state that Enceladus' ice is indeed pure H_2O , newer investigations tend to assume the existence of very small portions of other substances, see Matson *et al.* (2007). However, even in the latter case, the above value for ρ seems reasonable. Furthermore, the acceleration due to gravity on Enceladus is set to $g=0.079$ m s^{-2} .

The Green-Naghdi theory of type III includes the two thermal conductivities k_1 and k_2 , to which we shall refer as the non-classical and classical thermal conductivities, respectively. Green and Naghdi (1991) do not narrow the ratio of k_1 and k_2 . Since they describe thermal conductivities (or at least something similar), they should be non-negative, *i.e.*, $k_1, k_2 \geq 0$. Having another look at the heat transfer equation of type III, Eq. (3), we see that if $k_1=0$, the remaining equation is equivalent to the classical heat transfer equation resulting from Fourier's law. Thus, the classical theory is fully incorporated in the Green-Naghdi theory of type III. The other extreme case, *i.e.*, $k_2=0$, leads to an undamped wave equation, and that is what Green and Naghdi refer to as type II. One of its properties is that the constitutive equations are usually chosen in such a way that they do not include any energy dissipation. Such a property might be reasonable for modelling the pure second sound phenomenon, but even in this special case, the debate whether or not energy is dissipated is still going on (Green and Naghdi 1993, Quintanilla and Straughan 2000).

Although no experimental data exist on energy dissipation during the eruption of a cryovolcano on Enceladus, one can certainly conclude that the model should include energy dissipation due to the experiences on Earth, and due to the fact that so far a pure thermal wave propagation has only been proven below 20 K. We therefore identify the classical thermal conductivity k_2 with the measured thermal conductivity given in Eq.(5)₁,

$$k_2(T) = \frac{615}{T} \text{Wm}^{-1}\text{K}^{-1}. \quad (6)$$

For the non-classical thermal conductivity k_1 , we assume that it is proportional to k_2 ,

$$k_1(T) = \frac{k_2(T)}{t_{\text{proc}}} \times f, \quad (7)$$

where t_{proc} is a time-scale for the modelled process, and f is an adjustable, dimensionless factor. It is clear that, for small values of f , the Fourier-type (diffusive) heat flux will be dominant, while for large values of f , heat transport will be governed mainly by the non-classical $\nabla\alpha$ -type flux.

In order to constrain possible values for the non-classical thermal conductivity k_1 , we employ the following line of argumentation. One of the benefits of

the thermoelastic theory of Green and Naghdi is that it is capable of modelling the physical low temperature phenomenon of second sound. For materials which show this phenomenon, there exists a slower thermal wave called “second sound” in addition to the well-known mechanical (elastic) wave termed “first sound”. The velocity of the thermal wave was found to be typically about $\sqrt{3}$ times smaller than the velocity of the elastic wave (Bargmann and Steinmann 2005, 2006). If we apply this approximation for ice, we obtain an independent estimate for the value of k_1 ,

$$\begin{aligned} v_{\text{thermal}} &\approx v_{\text{elastic}} / \sqrt{3} \\ \Rightarrow \sqrt{\frac{k_1}{\rho c}} &\approx \sqrt{\frac{E}{\rho}} / \sqrt{3} \\ \Rightarrow k_1 &\approx \frac{Ec}{3}. \end{aligned} \quad (8)$$

For 100 K, this yields $k_1 = 2.9 \times 10^{12} \text{ W m}^{-1} \text{ K}^{-1}$, while $k_2 = 6.15 \text{ W m}^{-1} \text{ K}^{-1}$. If we choose the process time-scale as $t_{\text{proc}} = 1 \text{ d} = 86400 \text{ s}$ (see below), we obtain a factor f as large as $f = 4 \times 10^{16}$. However, since it is not likely that ice shows fully developed second-sound phenomena (otherwise it would most likely have been observed already), we argue that reasonable values for f must be at least several orders of magnitude smaller.

4.2 Computational domain, initial and boundary conditions

As a simplified representation of a cryovolcano and its environment on Enceladus, we consider a two-dimensional domain of 50 km (approx. 10 degrees of latitude) length and 500 m thickness, with the volcanic vent at the right edge. The problem is supposed to be symmetric around the vent, and the curvature of the surface is neglected. We assume that the water chamber next to the volcanic pipe is 1 km long and over-pressurized by a factor of 10 compared to the hydrostatic pressure of the ice. The set-up is illustrated in Fig. 3.

The initial conditions at the time $t_0 = 0$ are a surface temperature of 85 K (see Fig. 1 and its discussion in the introduction) and a bottom temperature of 273 K. The reference temperature T_0 required for the solution of the heat transfer equation (3) is set to the initial surface temperature, that is, $T_0 = 85 \text{ K}$. The simulated eruption starts abruptly at this time and lasts until $t = 1 \text{ d}$. During the eruption period, the temperature over the entire depth of the volcanic vent is set to 273 K, and the pressure in the vent falls linearly from the over-pressurized water chamber at the bottom to the zero value at the surface. At $t = 1 \text{ d}$, the eruption is “switched off”, and the computation is continued until $t_f = 10 \text{ d}$. For the process time-scale t_{proc} in Eq. (7), we choose the duration of the eruption, that is, $t_{\text{proc}} = 1 \text{ d}$.

There are no data available on the duration of a real eruption, so that the choice of one day is arbitrary. However, the general development of the heat

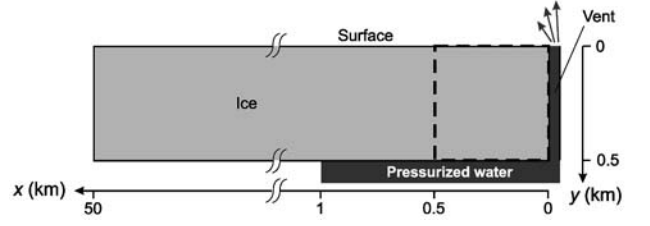


Fig. 3. Set-up of the model cryovolcano. The adjacent ice layer is 50 km long and 500 m thick. The dashed square marks the 500 m \times 500 m area next to the volcanic vent for which the evolution of the temperature field will be plotted in Figs. 4–7.

propagation will not be affected by the eruption time. Here, we want to discuss the effect of the Green-Naghdi model, and therefore, we do not focus on details of the temporal evolution.

The surface temperature T_s is computed from a radiation balance, which takes into account the incoming solar radiation, the black-body radiation from the ice surface and the geothermal heat flux approaching the ice surface from below. It reads

$$-S_0[1-A] + 4\sigma_{\text{SB}}T_s^4 - 4q_y = 0, \quad (9)$$

where S_0 is the solar constant for Enceladus, A the albedo (reflexivity of the ice surface), σ_{SB} the Stefan-Boltzmann constant ($5.67 \times 10^{-8} \text{ W m}^{-2} \text{ K}^{-4}$) and q_y the upward geothermal heat flux. As already mentioned in the introduction, the albedo is as high as 0.99, which is the highest value of any known body in our solar system (Buratti *et al.* 1990). The solar constant can be computed from its terrestrial counterpart, $S_{0,\text{Earth}} = 1368 \text{ W m}^{-2}$, via

$$S_0 = S_{0,\text{Earth}} \frac{r_{\text{SE}}^2}{r_{\text{SS}}^2} = 14.9 \text{ W m}^{-2}, \quad (10)$$

where r_{SE} and r_{SS} are the distances Sun-Earth (1 AU) and Sun-Saturn (9.58 AU), respectively. Note also that the assumed thickness of the ice layer of 500 m can be justified by inserting a surface temperature of 85 K and a bottom temperature of 273 K into the radiation balance (9) and expressing the heat flux with the classical (Fourier-type) part of Eq. (14)₂ as $q_y = -k_2 \partial T / \partial z$.

5. Results and discussion

The dimensionless factor f in Eq. (7) still needs to be specified. Since the available data on Enceladus do not give a hint on how to choose f in the first place, we have decided to vary this parameter starting with $f = 1$ and going up to $f = 10^8$. As mentioned above, for small values of f , our model will be close to the classical, Fourier-type heat conduction. By increasing f , the model will become more and more non-classical because of the increasing impact of the $\nabla\alpha$ -type flux. However, note that the maximum value $f = 10^8$ is still eight orders of magnitude smaller than the estimate

given in the discussion of Eq. (8), so that in neither case we assume fully developed second-sound properties for ice.

In the following, the solutions for $f=1$ (“case 1”), $f=10^6$ (“case 2”), $f=10^7$ (“case 3”) and $f=10^8$ (“case 4”) will be discussed. All simulations have been carried out with a numerical time-step of $\Delta t=10^{-3}$ d=1.44 min.

Figures 4–7 illustrate the temperature development of the $500\text{ m}\times 500\text{ m}$ square next to the volcanic pipe. The solutions are plotted at four different times of the observation for each of the four cases. First, the temperature is depicted right after the beginning of the volcanic eruption (*i.e.*, at time $t=1.44$ min). The next plot shows the temperature distribution 1 hour and 12 minutes after the beginning of the volcanic eruption — at that time the volcano is still erupting. Immediately after the end of the eruption, *i.e.*, after 1 day, we look at the temperature solution for the third time. Fourth, the temperature is plotted 10 days after the beginning of the eruption, that is, 9 days after its end.

In case 1, which is very close to the classical

Fourier approach, no change in temperature can be seen, see Fig. 4. Neither the 1-day-lasting volcanic eruption nor the cooling down period of 9 days have any noticeable impact on the temperature distribution within the ice.

In case 2, where $f=10^6$, hardly any changes in temperature can be seen during the volcanic eruption, see Fig. 5. However, 9 days after the end of the eruption, it can be clearly seen that the temperature in the volcanic pipe is decreasing, starting at the top, *i.e.*, at Enceladus’ surface.

Figures 6 and 7 show that, with an increasing impact of the non-classical $\nabla\alpha$ -type flux (cases 3 and 4), the volcanic eruption starts to heat the interior of the ice next to the pipe, and the surface temperature rises. Also, immediately after the end of the eruption, the ice starts to cool down, which is best visible in the volcanic pipe next to the surface. Depending on the dimensionless factor f , the ice temperature equilibrates slower or faster: The higher the value of f , the faster the system equilibrates. Furthermore, due to the increasing impact of the $\nabla\alpha$ -type heat flux,

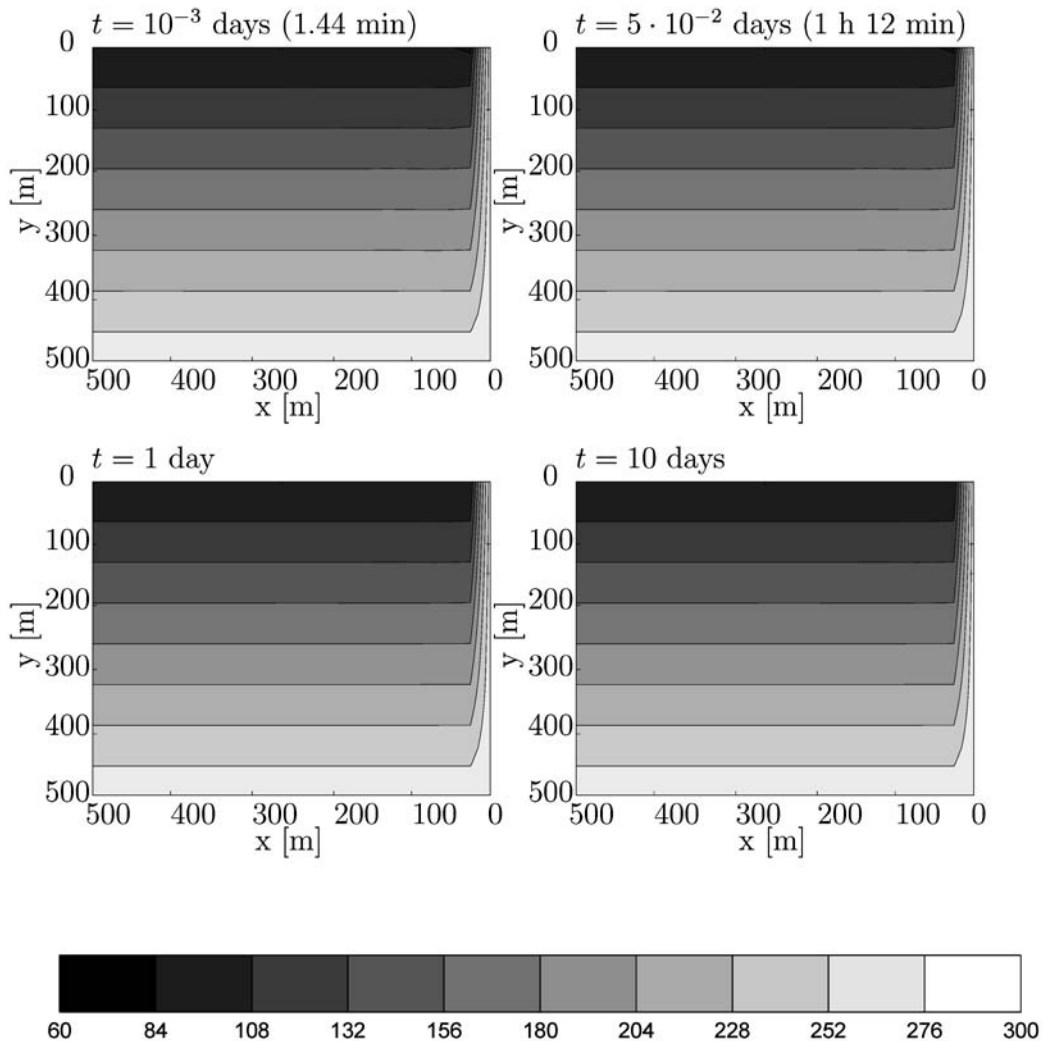


Fig. 4. Case 1 ($f=1$): Evolution of the temperature field (in K) in the $500\text{ m}\times 500\text{ m}$ area next to the volcanic vent shown in Fig. 3.

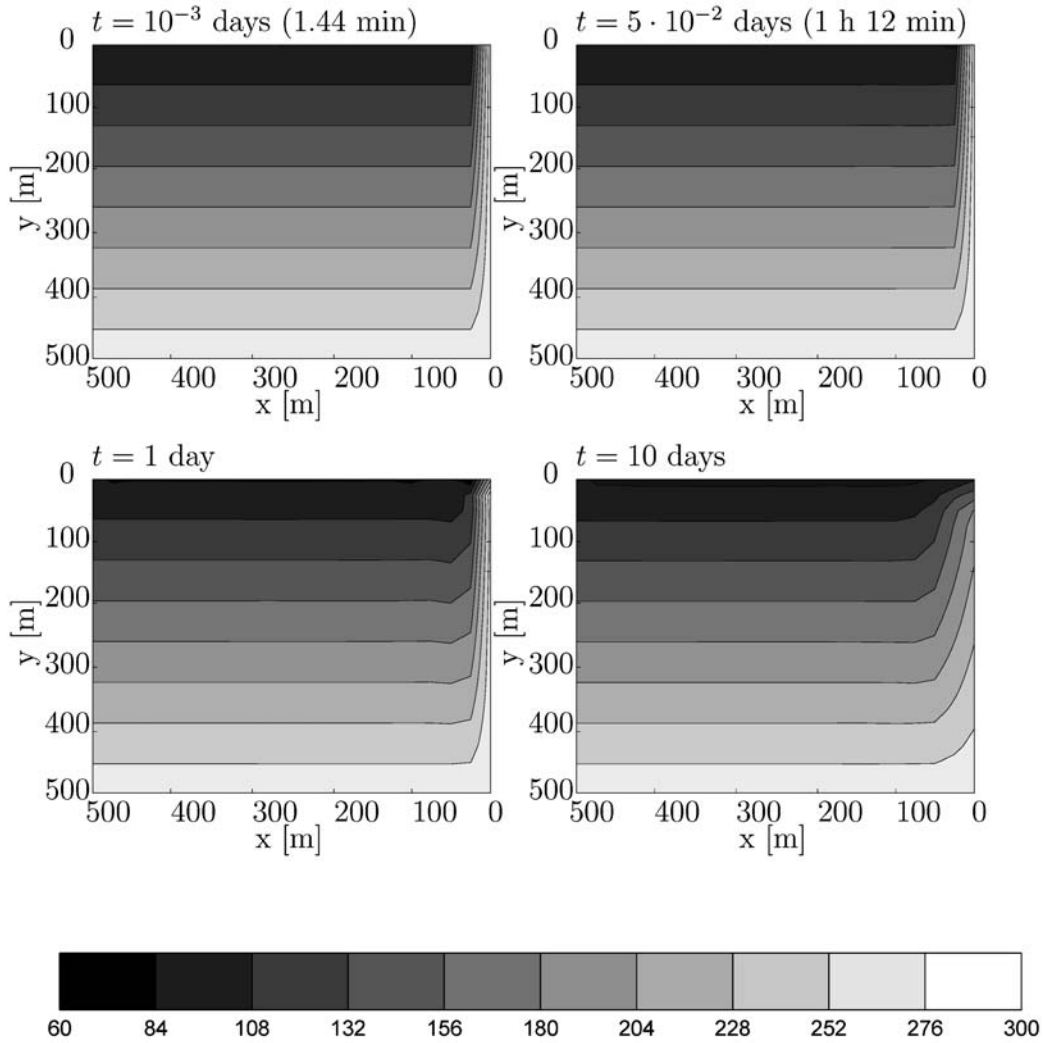


Fig. 5. Case 2 ($f=10^6$): Evolution of the temperature field (in K) in the $500\text{ m} \times 500\text{ m}$ area next to the volcanic vent shown in Fig. 3.

the temperature rises within the ice during the eruption. Owing to the radiation balance (9), the temperature change is most pronounced in the interior of the ice layer and smaller at the surface; however, a surface warming of the order of several degrees occurs in the vicinity of the vent during the eruption and fades away afterwards.

Spencer *et al.* (2006) discuss the temperature on Enceladus' surface observed during the Cassini flybys in 2005 based on infrared spectrometry. High-resolution data reveal that the occurrence of high temperatures is spatially correlated with the geological features termed “tiger stripes” (linear troughs), which are most likely the source of the cryomagma delivered during the volcanic eruptions. With regard to the results of our simulations, it is particularly interesting that the data also indicate some increased thermal emission from regions adjacent to the warm troughs (several kilometers away). This spreading of surface warming agrees roughly with the results of our cases 3 and 4, where the non-classical, $\nabla\alpha$ -type

heat flux contributes significantly to the heat transfer in the ice. By contrast, in case 1, which is very close to the classical Fourier approach, the warming extends to only a few meters away from the volcanic pipe during the simulation time (and is therefore invisible in Fig. 4). Of course, this depends on the assumed duration of the eruption, but the time-scale $[t]$ for purely diffusive heat transport over a length-scale of $[L]=1\text{ km}$ is as large as $[t]=\rho c [L]^2/k_2 \approx 4000\text{ a}$ (computed for 100 K), and it appears unlikely that a stationary cryovolcanic eruption can be sustained over such a long time. Therefore, with all due caution arising from our simplified model and the data uncertainties, it seems that non-classical heat transport in ice at cryogenic temperatures may play a role in explaining the observed temperature distribution in the vicinity of the volcanically active troughs in Enceladus' south polar region.

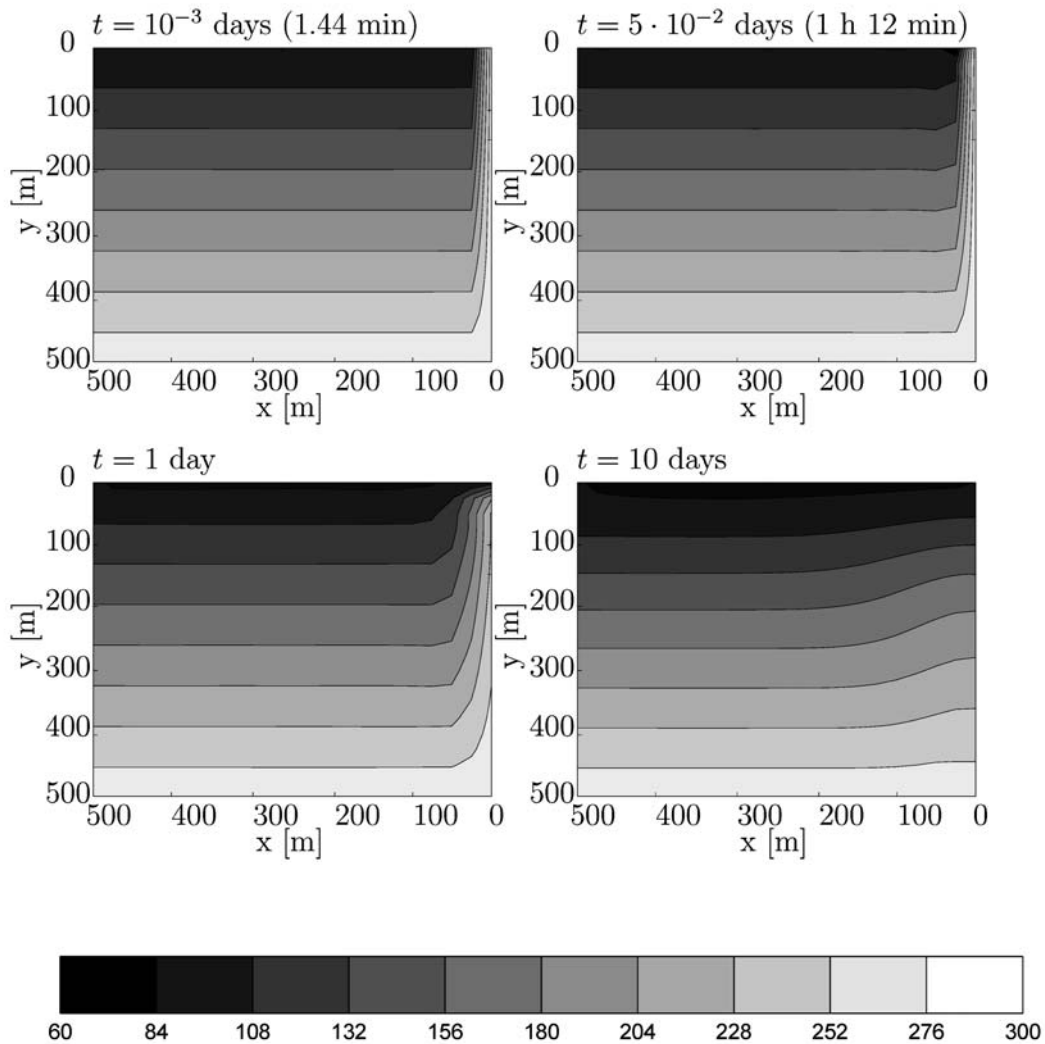


Fig. 6. Case 3 ($f=10^7$): Evolution of the temperature field (in K) in the $500\text{ m} \times 500\text{ m}$ area next to the volcanic vent shown in Fig. 3.

6. Conclusions

Motivated by the fully consistent and very general thermoelastic theory of Green and Naghdi (1991), the aim of this contribution was the modelling of cryovolcanism on Enceladus according to their approach. Since their theory of type III includes the classical thermoelastic theory as a limiting case ($k_1=0$) and allows for various non-classical models, we stick to this Green-Naghdi sub-theory. Type III allows thermal waves to propagate without energy dissipation at finite speed, another limiting case. We modeled cryovolcanism on Enceladus applying different scenarios lying in between the two extreme cases aforementioned.

First, we reiterated the basic equations of thermoelasticity based on the approach of Green and Naghdi. Second, we introduced a finite element method for the discretization of the governing system of equations. This is followed by a detailed description of the ap-

plied ice volcano model. Finally, we present numerical results for the Green-Naghdi theory type III for four different cases with increasing influence of the non-classical heat flux. While the approach closest to the classical theory (our case 1) does not allow for any significant spreading of surface warming away from the active volcanic vents, the scenarios where the non-classical heat flux plays a role (cases 3 and 4) show surface warming of several degrees in the vicinity of the vents. This seems to be in better agreement with temperature data based on infrared spectrometry (Spencer *et al.* 2006). Therefore, we tentatively and carefully conclude that a heat transport modelled by a more general approach than Fourier's *may* be significant in ice at the very low temperatures which occur on Enceladus and other icy moons in the outer solar system. Of course, complementary laboratory studies would be required in order to further support this idea.

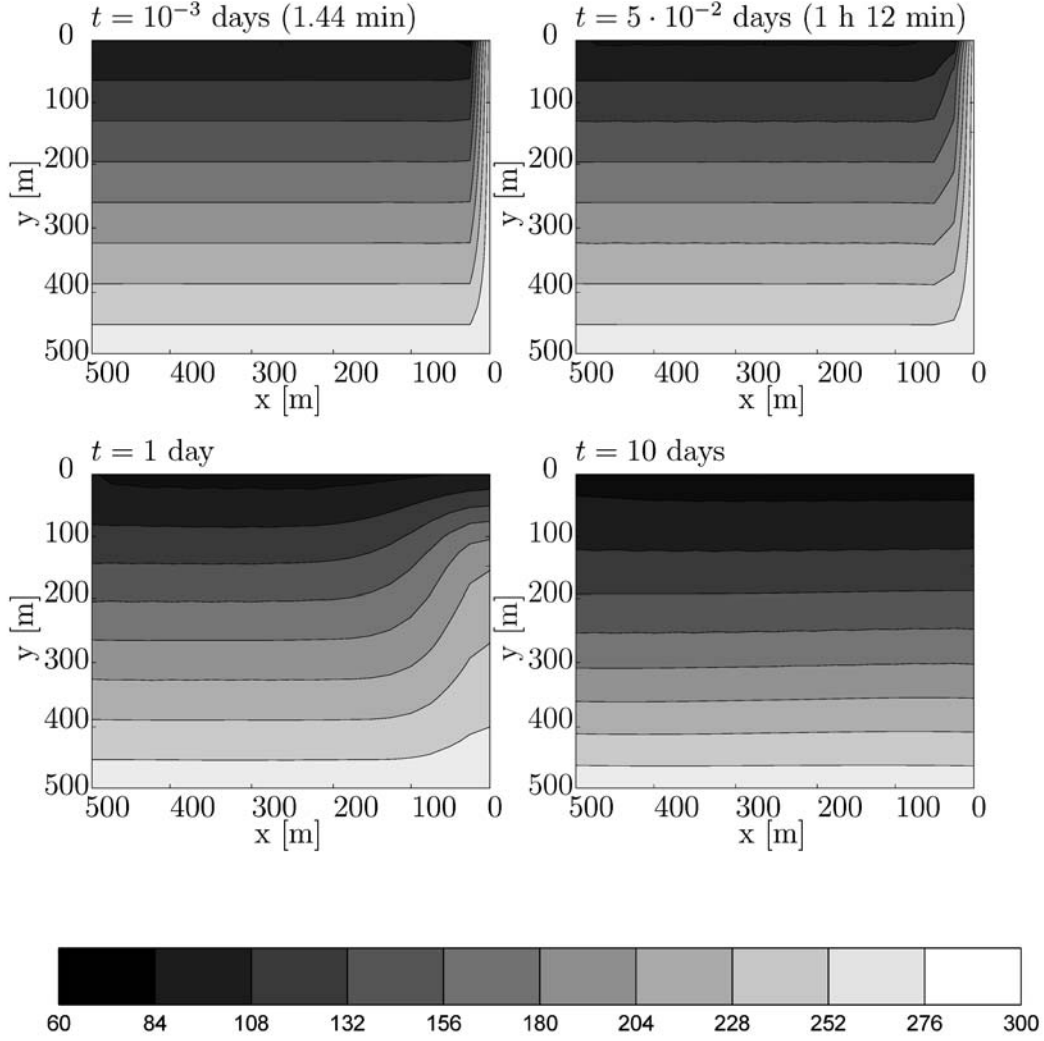


Fig. 7. Case 4 ($f=10^8$): Evolution of the temperature field (in K) in the $500\text{ m} \times 500\text{ m}$ area next to the volcanic vent shown in Fig. 3.

Appendix

Derivation of the governing equations for thermoelasticity of Green-Naghdi type III

The heat transfer equation (Eq. (3)) follows from the balance of entropy

$$\rho\dot{\eta} = -\text{div}\mathbf{h} + \rho[s + \xi], \quad (11)$$

where η , \mathbf{h} , s and ξ denote the specific entropy (entropy per mass unit), the entropy flux vector, the external entropy source and the internal rate of entropy production, respectively. Bargmann and Steinmann (2007) have shown that the classical thermodynamic relation between the entropy flux vector \mathbf{h} and the heat flux vector \mathbf{q} ,

$$T\mathbf{h} = \mathbf{q}, \quad (12)$$

can be transferred to the non-classical case.

As mentioned above, one of the main features of Green and Naghdi's theory of type III is the introduction of a new thermal variable, namely the thermal

displacement α . In case of geometrically linear thermoelasticity of type III, the specific free energy (free energy per mass unit) ϕ and the heat flux vector \mathbf{q} depend on the thermal displacement α , the temperature T , the thermal displacement gradient $\nabla\alpha$, the temperature gradient ∇T and the mechanical strain tensor $\boldsymbol{\varepsilon}$,

$$\begin{aligned} \phi &= \phi(\alpha, T, \nabla\alpha, \nabla T, \boldsymbol{\varepsilon}), \\ \mathbf{q} &= \mathbf{q}(\alpha, T, \nabla\alpha, \nabla T, \boldsymbol{\varepsilon}). \end{aligned} \quad (13)$$

The relations for ϕ and \mathbf{q} , based on those concluded by Green and Naghdi (1991), read

$$\begin{aligned} \rho\phi &= \frac{1}{2}\boldsymbol{\varepsilon} : \mathbf{E} : \boldsymbol{\varepsilon} - 3[T - T_0]\omega K \mathbf{I} : \boldsymbol{\varepsilon} \\ &\quad - \frac{\rho c}{T_0} \frac{[T - T_0]^2}{2} - [T - T_0]\rho\eta_0, \\ \mathbf{q} &= -[k_1\nabla\alpha + k_2\nabla T], \end{aligned} \quad (14)$$

where η_0 is the reference value of the specific entropy for $T=T_0$ and $\boldsymbol{\varepsilon}=\mathbf{0}$. The nonnegative specific heat capacity c is equal to $c=T\partial\eta/\partial T$. Moreover, the entropy reads

$$\rho\eta = -\frac{\partial(\rho\psi)}{\partial T} = \frac{\rho c}{T_0} [T - T_0] + 3\omega K \mathbf{I} : \boldsymbol{\varepsilon} + \rho\eta_0, \quad (15)$$

and the internal rate of entropy production ξ equals

$$\rho T \dot{\xi} = -\mathbf{h} \cdot \nabla T; \quad (16)$$

see Bargmann and Steinmann (2007). Thus, energy is dissipated during general processes.

The heat transfer equation of type III is derived by inserting the constitutive assumptions (14) and the relations (15) and (16) into Eq. (11) and, following Green and Naghdi (1993), subsequent replacement of T by T_0 . After some calculations, we finally obtain

$$\rho c \dot{T} = \text{div}(k_1 \nabla \alpha) + \text{div}(k_2 \nabla T) + \rho r - 3T_0 \omega K \mathbf{I} : \dot{\boldsymbol{\varepsilon}}, \quad (17)$$

where the heat source r is related to the external entropy source s via $r = Ts$.

The balance of linear momentum states that the rate of change of the momentum $\rho \dot{\mathbf{u}}$ is equal to the sum of the divergence of the Cauchy stresses $\boldsymbol{\sigma}$ and the volume force \mathbf{b} ,

$$\rho \dot{\mathbf{u}} = \text{div} \boldsymbol{\sigma} + \mathbf{b}. \quad (18)$$

The stresses $\boldsymbol{\sigma}$ are thermodynamically conjugated to the strains $\boldsymbol{\varepsilon}$ via the specific free energy ψ ,

$$\boldsymbol{\sigma} = \frac{\partial(\rho\psi)}{\partial \boldsymbol{\varepsilon}}. \quad (19)$$

Thus, the constitutive equation for the stresses reads

$$\boldsymbol{\sigma} = \mathbf{E} : \boldsymbol{\varepsilon} - 3[T - T_0] \omega K \mathbf{I}, \quad (20)$$

including thermo-mechanical coupling due to the last term. Inserting Eq. (20) into the balance of momentum (18) finally yields Eq. (4),

$$\rho \dot{\mathbf{u}} = \text{div}(\mathbf{E} : \boldsymbol{\varepsilon} - 3[T - T_0] \omega K \mathbf{I}) + \mathbf{b}. \quad (21)$$

Acknowledgments

The authors wish to thank N. Azuma and an anonymous referee who provided many helpful comments and suggestions. This work was supported by the German Research Foundation (Deutsche Forschungsgemeinschaft, DFG) under grant STE 544/23. Parts of the work (mainly the numerical simulations) were carried out during a visit of S.B. at the Institute of Low Temperature Science in Sapporo, supported by a research fellowship from the Japan Society for the Promotion of Science (JSPS).

References

Bargmann, S. and P. Steinmann. 2005. Finite element approaches to non-classical heat conduction in solids. *Comp. Meth. Eng. Sci.*, **9** (2), 133–150.

- Bargmann, S. and P. Steinmann. 2006. Theoretical and computational aspects of non-classical thermoelasticity. *Comp. Meth. Appl. Mech. Eng.*, **196** (1–3), 516–527.
- Bargmann, S. and P. Steinmann. 2007. Classical results for a non-classical theory: remarks on thermodynamic relations in Green-Naghdi thermo-hyperelasticity. *Cont. Mech. Thermodyn.*, **19** (1–2), 59–66.
- Bargmann, S. and P. Steinmann. 2008. An incremental variational formulation of dissipative and non-dissipative coupled thermoelasticity for solids. *Heat and Mass Transfer*, **45**, 107–116. doi: 10.1007/s00231-008-0405-5.
- Bargmann, S., P. Steinmann and P.M. Jordan. 2008. On the propagation of second sound in linear and nonlinear media: Results from Green-Naghdi theory. *Phys. Lett. A*, **372** (24), 4418–4424.
- Buratti, B.J., J.A. Mosher and T. V. Johnson. 1990. Albedo and color maps of the Saturnian satellites. *Icarus*, **87** (2), 339–357.
- Collins, G.C. and J.C. Goodman. 2007. Enceladus' south polar sea. *Icarus*, **198** (1), 72–82.
- Eriksson, K., D. Estep, P. Hansbo and C. Johnson. 1996. *Computational differential equations*. Studentlitteratur, Lund, Sweden.
- Green, A.E. and P.M. Naghdi. 1991. A reexamination of the basic postulates of thermomechanics. *Proc. R. Soc. Lond. A*, **432** (1885), 171–194.
- Green, A.E. and P.M. Naghdi. 1993. Thermoelasticity without energy dissipation. *J. Elasticity*, **31** (3), 189–208.
- Greve, R. 2006. Fluid dynamics of planetary ices. *GAMM-Mitteilungen*, **29** (1), 29–51.
- Kieffer, S.W., X. Lu, C.M. Bethke, J.R. Spencer, S. Marshak and A. Navrotsky. 2006. A clathrate reservoir hypothesis for Enceladus' south polar plume. *Science*, **314** (5806), 1764–1766.
- Kumar, R. and S. Deswal. 2001. Disturbance due to mechanical and thermal sources in a generalized thermo-microstretch elastic half space. *Sadhana*, **26** (6), 529–547.
- Matson, D.L., J.C. Castillo, J. Lunine and T.V. Johnson. 2007. Enceladus' plume: Compositional evidence for a hot interior. *Icarus*, **187** (2), 569–573.
- Nimmo, F., J.R. Spencer, R.T. Pappalardo and M.E. Mullen. 2007. Shear heating as the origin of the plumes and heat flux on Enceladus. *Nature*, **447** (7142), 289–291.
- Porco, C.C., P. Helfenstein, P.C. Thomas, A.P. Ingersoll, J. Wisdom, R. West, G. Neukum, T. Denk, R. Wagner, T. Roatsch, S. Kieffer, E. Turtle, A. McEwen, T.V. Johnson, J. Rathbun, J. Veverka, D. Wilson, J. Perry, J. Spitale, A. Brahic, J.A. Burns, A.D. DelGenio, L. Dones, C.D. Murray and S. Squyres. 2006. Cassini observes the active south pole of Enceladus. *Science*, **311** (5766), 1393–1401.
- Powell, R.W. 1958. Preliminary measurements of the thermal conductivity and expansion of ice. *Proc. R. Soc. Lond. A*, **247** (1251), 464–466.
- Puri, P. and P.M. Jordan. 2004. On the propagation of plane waves in type-III thermoelastic media. *Proc. R. Soc. Lond. A*, **460** (2051), 3203–3221.
- Quintanilla, R. and B. Straughan. 2000. Growth and uniqueness in thermoelasticity. *Proc. R. Soc. Lond. A*, **456** (1998), 1419–1429.
- Slack, G.A. 1980. Thermal conductivity of ice. *Phys. Rev. B*, **22** (6), 3065–3071.
- Spencer, J.R., J.C. Pearl, M. Segura, F.M. Flasar, A. Mamoutkine, P. Romani, B.J. Buratti, A.R. Hendrix, L.J. Spilker and R. M.C. Lopes. 2006. Cassini encounters Enceladus: Background and the discovery of a south polar hot spot. *Science*, **311** (5766), 1401–1405.